sustainability

MDPI

Article

Influence of Dissolved Oxygen and Temperature on Nitrogen Transport and Reaction in Point Bars of River

Xunchuan Song [1], Ying Liu [1,*], Jinghong Feng [1], Defu Liu [1], Qilin Yang [2], Ziyan Lu [1] and Huazhen Xiao [1]

[1] Key Laboratory of Intelligent Health Perception and Ecological Restoration of Rivers and Lakes, Ministry of Education, Hubei University of Technology, Wuhan 430068, China
[2] Institute of Geo-Environment Monitoring of GuiZhou Province, Guiyang 550001, China
* Correspondence: liuy@hbut.edu.cn

Abstract: Point bars are crucial elements of river systems, significantly enhancing the nitrogen cycle in riparian zones by facilitating hyporheic exchange between surface water and riparian zones. This study investigated the impact of dissolved oxygen (DO) concentration and temperature on nitrogen transport and reactions in river point bars. A two-dimensional coupled surface water–groundwater model was developed to analyze nitrogen distribution, variations, and reaction rates in rivers with point bars. The model considered three chemical reactions controlling nitrogen transformation: aerobic respiration, nitrification, and denitrification, with DO and temperature as independent variables. The results indicated that DO variations have a limited effect on solute migration depth, whereas increased temperature reduces solute migration depth. At surface water DO concentrations of 0.1, 0.2, and 0.4 mol/m^3, nitrate removal in the riparian zone was 0.022, 0.0064, and 0.0019 mol/m, respectively. At riparian temperatures of 5 °C, 15 °C, and 25 °C, nitrate removal was 0.012, 0.041, and 0.16 mol/m, respectively. Nitrogen removal is more sensitive to temperature variations than to changes in DO concentration. In this research, the decrease in DO concentrations and the temperature increase greatly enhanced the riparian zone's denitrification effect. This study improves our understanding of how riparian zones impact nitrogen cycling under various environmental conditions.

Keywords: point bars; dissolved oxygen; temperature; denitrification; riparian zone; river ecological restoration

Citation: Song, X.; Liu, Y.; Feng, J.; Liu, D.; Yang, Q.; Lu, Z.; Xiao, H. Influence of Dissolved Oxygen and Temperature on Nitrogen Transport and Reaction in Point Bars of River. *Sustainability* **2024**, *16*, 8208. https://doi.org/10.3390/su16188208

Academic Editor: Giuseppe Barbaro

Received: 25 July 2024
Revised: 6 September 2024
Accepted: 19 September 2024
Published: 20 September 2024

1. Introduction

Point bars are distinct features adjacent to rivers that expand riparian zones and connect aquatic and terrestrial ecosystems [1]. Point bars modify the local hydraulic gradient in river channels, promoting hyporheic exchange between river water and riparian groundwater. This process is essential for intercepting river nutrients, improving water quality, and supporting healthy river ecosystems [2].

Hyporheic exchange (HE) driven by point bars actively transports dissolved oxygen (DO), nutrients, and microorganisms between river water and riparian zones, supporting nitrogen biogeochemical cycles in rivers and groundwater. This process is crucial for nitrogen transport and reactions, influencing its quantities and states within the river ecosystem [3]. In river restoration projects, artificially constructed gravel point bars significantly promote HE and achieve high nitrate removal efficiencies [4,5]. Simultaneously, point bars host diverse microbial communities that play vital roles in river biogeochemical cycles [6]. Therefore, point bars are essential to the functional integrity of river ecosystems, serving as pathways for inducing HE and enhancing denitrification during river purification processes.

Nitrogen is a key factor in eutrophication of water bodies. Excessive nitrogen leads to algal blooms, which severely degrade water quality and biodiversity. Riparian zones

reduce nitrogen concentrations in water via plant uptake, microbial transformation, and sediment fixation [7]. From a sustainable development perspective, the nitrogen removal capacity of riparian zones is vital for achieving environmental goals. Healthy riparian zones help maintain water quality and provide various ecological services, including water source protection, flood regulation, biodiversity maintenance, and climate regulation [8,9]. These ecological services are significantly valuable to the long-term well-being of human society. Therefore, protecting and restoring riparian zones is crucial for achieving sustainable development goals [10]. To enhance nitrogen removal efficiency, scientific research should explore the specific mechanisms and efficiencies of nitrogen removal under various environmental conditions, providing solid scientific evidence for environmental policies and management decisions.

In the nitrogen removal process in riparian zones, denitrification is considered the most effective mechanism [11]. Research indicates that over half of the nitrates entering river systems are removed by denitrification before discharge into the ocean [12].

Denitrification in riparian zones is influenced by environmental factors such as water flow rate, nitrogen sources, plants, pH, sediment properties, dissolved oxygen (DO), and temperature [13,14]. Increased water flow rates may enhance the conveyance and mixing of nitrogenous materials, hastening their transformation and elimination processes [15]. However, excessively high flow rates might cause erosion and loss of nitrogenous matter, limiting denitrification effectiveness [16]. Elevated nitrogen source concentrations may constrain the denitrification process, potentially giving rise to novel contaminants such as nitrite nitrogen. In nitrification, ammonia nitrogen is oxidized to nitrite, followed by its oxidation to nitrate. When nitrogen source concentrations are too high, nitrite formation may outpace oxidation, leading to nitrite accumulation in the system. This can be toxic to aquatic organisms in rivers and pose health risks in drinking water treatment [17–19]. Plant roots provide organic carbon sources for denitrifying microorganisms, promoting microbial activity, and accelerating denitrification. Additionally, plants influence soil moisture through transpiration, regulating soil redox conditions and affecting denitrification frequency and intensity. Plant roots also alter soil structure, increasing permeability and porosity, which enhances nitrogen transfer and transformation efficiency. The impact of plant species on denitrification varies based on root characteristics, growth rates, and soil moisture regulation ability [20]. An appropriate pH level facilitates the growth and metabolic activity of denitrifying microbes, enhancing denitrification efficiency. Generally, the optimal pH for denitrification is between 7 and 9. Excessively acidic or alkaline conditions can change enzyme conformation and activity, reducing their catalytic ability and denitrification rate [21,22]. Significant denitrification reactions have also been observed in rivers contaminated with acidic mine wastewater [23], indicating varied pH tolerances for different denitrification mechanisms. Sediment plays a dual role in the nitrogen cycle, serving as both a nitrogen reservoir and a site for transformation reactions [24,25]. Sediment organic content supplies carbon sources, fostering denitrification within the river substrate and serving as an effective nitrogen abatement mechanism [26]. However, sediments might also release nitrogen, particularly when exogenous nitrate loads to the fluvial system are reduced [27]. The physical characteristics of sediment, such as particle size, porosity, and depositional dynamics, affect nitrogen adsorption–desorption processes, indirectly regulating its bioavailability and biogeochemical transformations [28].

In riparian zones, DO is recognized as a pivotal factor influencing element cycling and pollutant degradation [29]. As a primary oxidizing agent, DO strongly influences nitrogen and carbon cycling [30]. These biogeochemical processes significantly affect water quality, microbial activities, and benthic habitats [31,32]. DO largely dictates the redox conditions that govern nitrification and denitrification timing and occurrence in riparian zones [33].

Temperature regulates microbial activity and biomass, determining denitrification efficiency and rate in riparian zones [34,35]. Temperature variations may affect oxygen diffusion and nutrient distribution, indirectly influencing microbial activity and efficiency [36,37]. Temperature also affects the growth of aquatic plants and animals, influencing riverine

biotic community structure, which may affect nitrogen migration and transformation in HZ [38,39]. Research indicates a strong negative relationship between surface water nitrate levels and river temperatures, suggesting higher temperatures reduce nitrate concentrations [40]. In stream sediments, denitrification at 25 °C is twice that at 8 °C, as higher temperatures increase denitrifying bacteria's metabolic rate within a certain range [41]. The promotive influence of temperature on bioprocesses has limits; overly high water temperatures can reduce the activity or cause mortality of denitrifying bacteria, suppressing denitrification [42,43]. Elevated temperatures may accelerate the mineralization of organic compounds, reducing their concentration and restricting the availability of electron donors in denitrification [44,45].

While point bars are widespread in natural rivers and used in restoration projects, studies on the effects of DO and temperature on nitrogen migration and transformation in point bars are scarce. Temperature and DO are key abiotic factors regulating nitrogen removal in river systems. Understanding the influence of these factors on nitrogen removal is crucial for efficient river management and water quality enhancement.

Numerical simulation, a crucial method for studying river nitrogen cycling, quantitatively describes the continuous behavior of nitrogen migration and transformation in groundwater. This paper develops a two-dimensional surface water–groundwater coupled model to study nitrogen cycling in point bars. Similar models are widely cited. For example, Bardini et al. used a numerical model to simulate turbulent water flow and pressure distribution over dunes, evaluating the flow field and biogeochemical reactions in hyporheic sediments [46]. Zheng et al. used this model to analyze nitrogen migration and transformation in polluted and natural rivers [47,48]. Pin et al. used the model to examine the impact of bioclogging on nitrate source-sink functions in the hyporheic zone [49].

This study aims to quantify the effects of DO and temperature on removal processes in riparian zones with point bars using numerical simulation. The findings play a significant guiding role in applying point bars in river ecological restoration under different environmental scenarios.

2. Materials and Methods

2.1. Conceptual Model

To simulate the phenomena of water flow movement, solute migration, and chemical reactions in the HZ and analyze nitrogen cycling within a point bar, this study employed the commercial finite element software COMSOL Multiphysics (6.2, COMSOL Inc., Stockholm, Sweden) to develop a two-dimensional model coupling surface water–groundwater interactions and multi-component reactive solute transport (Figure 1).

The interaction between river water and the riverbank is conceptualized in Figure 1. The riverbank is simplified as a plane, with the right side of the river used for modeling [50]. Surface water, abundant in nutrients and DO, undergoes local pressure variations as it flows, due to hindrances from the riverbanks, leading to an uneven distribution of pressure that compels the surface water to seep into the riverbanks and initiate nitrogen biogeochemical reactions within [51]. The interface between the river water and the bank sediments is known as the Water–Sediment Interface (WSI), which exists as a mixed boundary in the model, functioning as both a pressure and concentration input boundary [46–49]. Given the potential complexity of dynamic temperature effects, we assumed uniform and stable temperatures for the point bar [47].

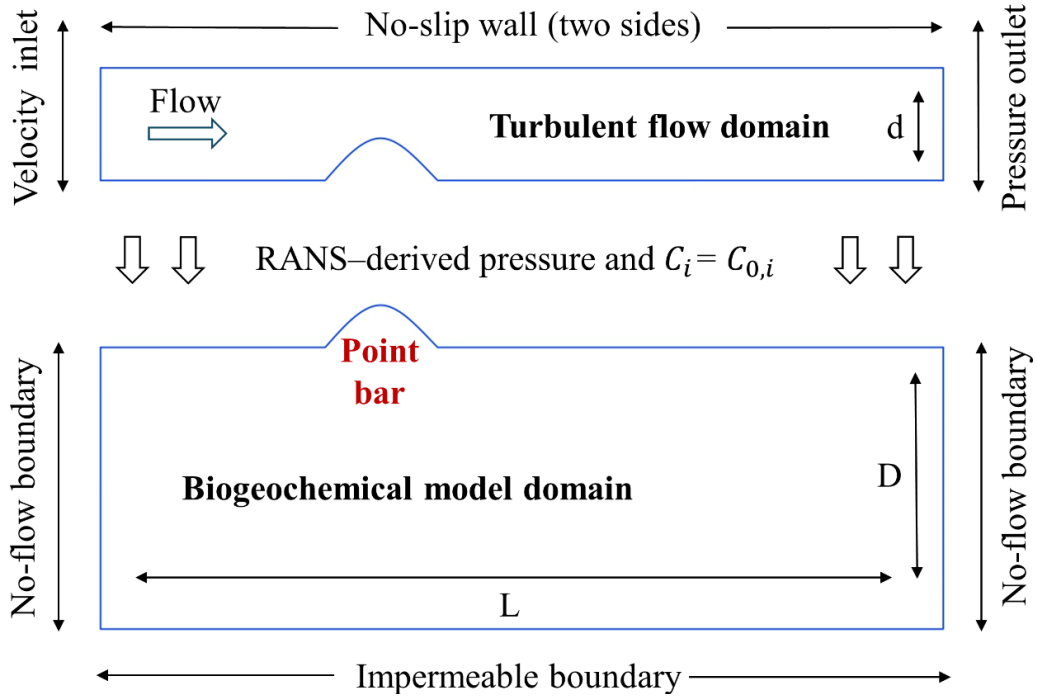

Figure 1. Modeling scheme. Upper part describes the pressure, velocity, and wall boundary conditions of the river flow turbulence model; lower part displays the pressure and concentration boundary conditions for the solute reactive transport in the porous medium. The model domain represents a riverbank with length L = 30 m and width D = 12 m (with a point bar 4 m long and 1.5 m wide, and the center of the bar 10 m from the leftmost edge of the riverbank), and a river channel of the same length as the riverbank and width of d = 4 m.

2.2. Governing Equations

2.2.1. Surface Water Flow

The flow of river water in nature is generally irregular, unsteady, and follows a chaotic and winding trajectory, typical of turbulent flow [52]. To simulate the turbulent process of surface water, this paper employs the RNG k-ε turbulence model to solve the Reynolds-averaged Navier–Stokes (RANS) equations. This model is widely recognized in industrial applications and more accurately depicts flows with high strain rates and significant streamline curvature [53].

The model requires solving for the turbulent kinetic energy k and its dissipation rate ε, with the equations formulated as follows:

$$\frac{\partial k}{\partial t} + \frac{\partial k u_i}{\partial x_i} = \frac{\partial}{\partial x_j}\left(D k_{eff} \frac{\partial_k}{\partial x_i}\right) + G_k - \varepsilon \quad (1)$$

$$\frac{\partial_\varepsilon}{\partial t} + \frac{\partial \varepsilon u_i}{\partial x_i} = \frac{\partial}{\partial x_i}\left(D \varepsilon_{eff} \frac{\partial \varepsilon}{\partial x_i}\right) + C_{1\varepsilon}\frac{\varepsilon}{k} G_k - C_{2\varepsilon}\frac{\varepsilon^2}{k} \quad (2)$$

u_i denotes the turbulent velocity; G_k corresponds to the generation of turbulent kinetic energy caused by the average velocity gradient; Dk_{eff} and $D\varepsilon_{eff}$ are the effective diffusivity for k and ε, respectively; and $C_{1\varepsilon}$ and $C_{2\varepsilon}$ are constants in the model [54].

This approach enables the simulation of steady-state mean unidirectional turbulent flow in river channels, yielding the river's velocity and pressure distributions. Moreover, this method has been validated, with the simulated pressure distribution along the wall interface closely aligning with experimental observations [55].

2.2.2. Groundwater Flow

Darcy's law can describe the free flow of fluids through porous media (such as sediments, sponges, activated carbon, etc.) [56]. Therefore, in the groundwater simulation part of this study, Darcy's law is chosen to simulate the movement of groundwater flow through sediments. The equation is as follows:

$$u = -\frac{\kappa}{\mu}\nabla p \tag{3}$$

κ is the permeability of the porous medium; μ is the dynamic viscosity of the fluid; and p is the pressure [57].

2.2.3. Multicomponent Reactive Transport

The transport and reaction of nitrogen in rivers involve complex coupling between groundwater flow, solute transport, and chemical reactions. Consequently, this study developed a multi-component solute reactive transport model, incorporating four key reactants: dissolved organic carbon (DOC), DO, nitrate (NO_3^-), and ammonium ion (NH_4^+). The model focused on their reactions and interconversions during groundwater movement.

This study did not specifically consider particulate organic carbon (POC), as POC particles could affect the permeability of sediments and the distribution of bacterial communities, potentially complicating the system too much for effective study [49,58]. Furthermore, this study did not consider the intrinsic nutrients in the riparian zone. It assumed that all nutrients originate solely from seepage inputs from the river water, simplifying the analysis and isolating the effects of the factors under investigation [47,49].

The multi-component solute reactive transport model incorporates three crucial biogeochemical reactions that govern nitrogen: nitrification (NI), denitrification (DN), and aerobic respiration (AR). As the majority of nitrogen in rivers is eliminated through DN, this article does not address other nitrogen transformation processes like ammonification, assimilation, or anaerobic ammonium oxidation. The expressions for the three key chemical reactions are shown in Table 1. To enhance the accuracy of the solution results, we employed a refined meshing approach, resulting in 113,616 free triangular elements.

Table 1. The reactions considered in the simulations.

Reaction Type	Expression
Aerobic respiration (AR)	$CH_2O + O_2 \rightarrow H_2O + CO_2$
Nitrification (NI)	$NH_4^+ + 2O_2 \rightarrow NO_3^- + H_2O + 2H^+$
Denitrification (DN)	$5CH_2O + 4NO_3^- + 4H^+ \rightarrow 7H_2O + 5CO_2 + 2N_2$

Given that nitrogen transformation and migration in riparian zone sediments involve several reactions, the groundwater model requires the incorporation of additional multi-component solute reaction transport equations. Hence, we incorporated a porous media solute transport module into the existing groundwater flow model. This module is coupled with the Darcy flow equations to simulate the nitrogen migration and transformation processes in the riparian zone. The porous media solute transport process follows the mass conservation equation, which is expressed as follows [59]:

$$\frac{\partial}{\partial t}(\theta_l c_i) + \frac{\partial}{\partial t}(\rho c_{P,i}) + \frac{\partial}{\partial t}(\theta_g c_{G,i}) + \boldsymbol{u}\cdot\nabla c_i = \nabla\cdot[(D_{D,i} + D_{e,i})\nabla c_i] + R_i + S_i \tag{4}$$

c_i is the concentration of species i in the liquid phase (mol/m^3), $c_{P,i}$ is the amount of species i adsorbed on the solid particles [mol/(ρ_s g)], and $c_{G,i}$ is the concentration of species i in the gas phase (mol/m^3);
$\frac{\partial}{\partial t}(\theta_l c_i)$, $\frac{\partial}{\partial t}(\rho c_{P,i})$, and $\frac{\partial}{\partial t}(\theta_g c_{G,i})$ are the transient concentration changes of the matter in the liquid, solid, and gas phases, respectively;

$u \cdot \nabla c_i$ indicates the convective transfer of matter under the action of the velocity field of the solvent; $\nabla \cdot [(D_{D,i} + D_{e,i}) \nabla c_i]$ describes three modes of mass transfer-mechanical diffusion, molecular diffusion, and volatilization in the gas phase, wherein D_D is the diffusion tensor (m^2/s), and D_e is the effective diffusion coefficient (m^2/s);
S_i is the source term and can describe the inflow or outflow of the species within a liquid; and R_i is an expression of the rate of reaction that can represent the chemical reactions of the species in the three phases [$mol/(m^3 \cdot s)$].

The net reaction rate expressions for these four key chemicals (DO, DOC, NO_3^-, and NH_4^+) are shown below [47]:

$$R_{DOC} = -k_{DOC} \cdot C_{DOC} \quad (5)$$

$$R_{NH_4^+} = -k_{NH_4^+} \cdot C_{NH_4^+} \cdot C_{O_2} \quad (6)$$

$$R_{O_2} = -f_1 \cdot k_{DOC} \cdot C_{DOC} \cdot \beta_1 - 2k_{NH_4^+} \cdot C_{NH_4^+} \cdot C_{O_2} \quad (7)$$

$$R_{NO_3^-} = -f_2 \cdot k_{DOC} \cdot C_{DOC} \cdot \beta_2 + k_{NH_4^+} \cdot C_{NH_4^+} \cdot C_{O_2} \quad (8)$$

C_{DOC}, $C_{NH_4^+}$, and C_{O_2} denote the concentrations of DOC, NH_4^+, and DO, respectively;
The terms k_{DOC} and $k_{NH_4^+}$ correspond to the reaction rate constants for DOC and NH_4^+, respectively;
The fractions f_1 and f_2 reflect the proportions of electrons consumed in the reduction of O_2 and NO_3^-, respectively;
β_1 is defined as the ratio of moles of electrons transferred per mole of DOC oxidized to the moles of electrons per mole of reducing agent in the aerobic respiration (AR) reaction;
And β_2 represents the ratio of moles of electrons transferred per mole of DOC oxidized to moles of electrons per mole of reducing agent in the NI reaction.

The key parameters of the multi-component solute reactive transport model are shown in Table 2, with concentrations of four reactants in rivers referring to Chinese surface water quality standards. It should be noted that when studying dissolved oxygen concentration as a single variable, the temperature of the point bar is maintained at 20 °C.

Table 2. Key parameters of a multi-component solute reactive transport model.

Parameters	Size	Unit	Ref.
Porosity	0.4		[50]
Hydraulic conductivity	30	m/d	[50]
Dispersity of longitude	0.1	m	[60]
Dispersity of transverse	0.01	m	[60]
Diffusion coefficient	10^{-9}	m^2/s	[61]
DO concentration in river	0.1, 0.2, 0.4	mol/m^3	
NO_3^- concentration in river	0.16	mol/m^3	[50]
NH_4^+ concentration in river	0.083	mol/m^3	[50]
DOC concentration in river	0.2	mol/m^3	[50]
Oxygen inhibition constant	0.03	mol/m^3	[47]
Point bar temperature	5, 15, 25	°C	

2.3. Response of Reaction Rate to Temperature

In chemical reactions, the rate constant is solely temperature-dependent, and its magnitude is a primary factor determining the reaction rate [62]. Nitrification (NI) and denitrification (DN), as bacterial-mediated biochemical reactions, are highly sensitive to temperature changes in the river [47,63]. Consequently, this paper establishes a response equation for nitrogen reactions to temperature, using the Arrhenius equation to quantitatively describe the relationship between temperature and reaction:

$$k(T) = Ae^{-E/RT} \quad (9)$$

$$k(T_1) = k(T_2)e^{-\frac{E}{R}(\frac{1}{T_1}-\frac{1}{T_2})} \quad (10)$$

where k is the rate constant; A is the Svante August Arrhenius constant; E is the activation energy; R is the gas constant; and T is the temperature.

2.4. Evaluated Indicators of Nitrogen Removal

Nitrate removal in the riparian zone can be quantitatively analyzed through integration. The nitrate removal per unit length of the riverbank can be represented by the following formula:

$$N_{DN} = \int_0^t \int_A \theta R_{NO_3^-} dAdt \quad (11)$$

where N_{DN} is the total nitrate consumption through DN per unit of riparian length; t is the total simulation time (48 h); A is the total area of the model domain; and $R_{NO_3^-}$ is the net reaction rate of nitrate [47,64].

The influx and efflux of species in the riparian zone adhere to a mass balance equation, with the influx and efflux amount of each species determinable via integration methods. The species influent amount per unit length can be calculated using the following equation:

$$A_{in} = \int_0^t \int_L C_{in} F_{tb} dLdt \quad (12)$$

where A_{in} represents the amount of the species entering the riverbank through subsurface flow from the upstream river per unit length; L is the total length of the top inflow boundary; C_{in} is the influent concentration of the species; and $F_{tb}dL$ represents the flux from the top inflow boundary into the riparian zone [47,50].

The species effluent amount per unit length can be calculated using the following equation:

$$A_{out} = \int_0^t \int_S C_{out} F_{tb} dSdt \quad (13)$$

where A_{out} represents the amount entering the downstream river through subsurface flow from the riverbank per unit length; S is the total length of the top outflow boundary; C_{out} is the effluent concentration of the species; and $F_{tb}dS$ represents the flux from the top outflow boundary into the river.

2.5. Field Tracer Experiment and Model Validation

The reliability and accuracy of the numerical simulations were validated using tracer technology for stability analysis. The experimental point bar was located in the Xiajiasi River, Huangpi District, Wuhan City, Hubei Province (114°28′ E, 31°02′ N). Three monitoring points were selected: upstream, mid-bar, and downstream along the riverbank.

A model replicating real river conditions was constructed in COMSOL. The domain point probe function was used to specify corresponding points in the solution domain, simulating tracer concentration changes at the monitoring points.

We conducted a tracking experiment, revealing that the root mean square error (RMSE) between the simulated and measured tracer concentrations at each monitoring point was consistently below 3.3%. Furthermore, all determination coefficients (R^2) exceeded 0.65 [47]. Consequently, this model is suitable for predicting changes in the groundwater dynamic field.

3. Results

3.1. Effect of DO Concentration on Nitrogen Transport and Reaction

Figure 2 illustrates the distribution of four key species concentrations and the rates of NI (nitrification) and DN (denitrification) reactions in the riparian zone under varying DO conditions. Overall, the four solutes (DO, NO_3^-, NH_4^+, and DOC) display a wavy band distribution, thicker in the center and tapering off towards the sides. The penetration

depth and concentration distribution of these solutes vary due to differences in their initial concentrations and the chemical reactions involved. Concentration peaks and the highest spatial reaction rates of NI typically occur at the left interface or the center of the bar, where HE is most intense [50]. The high flow rate resulting from the pressure difference in this area is the primary driving force behind the continuous migration and diffusion of solutes into the riverbank.

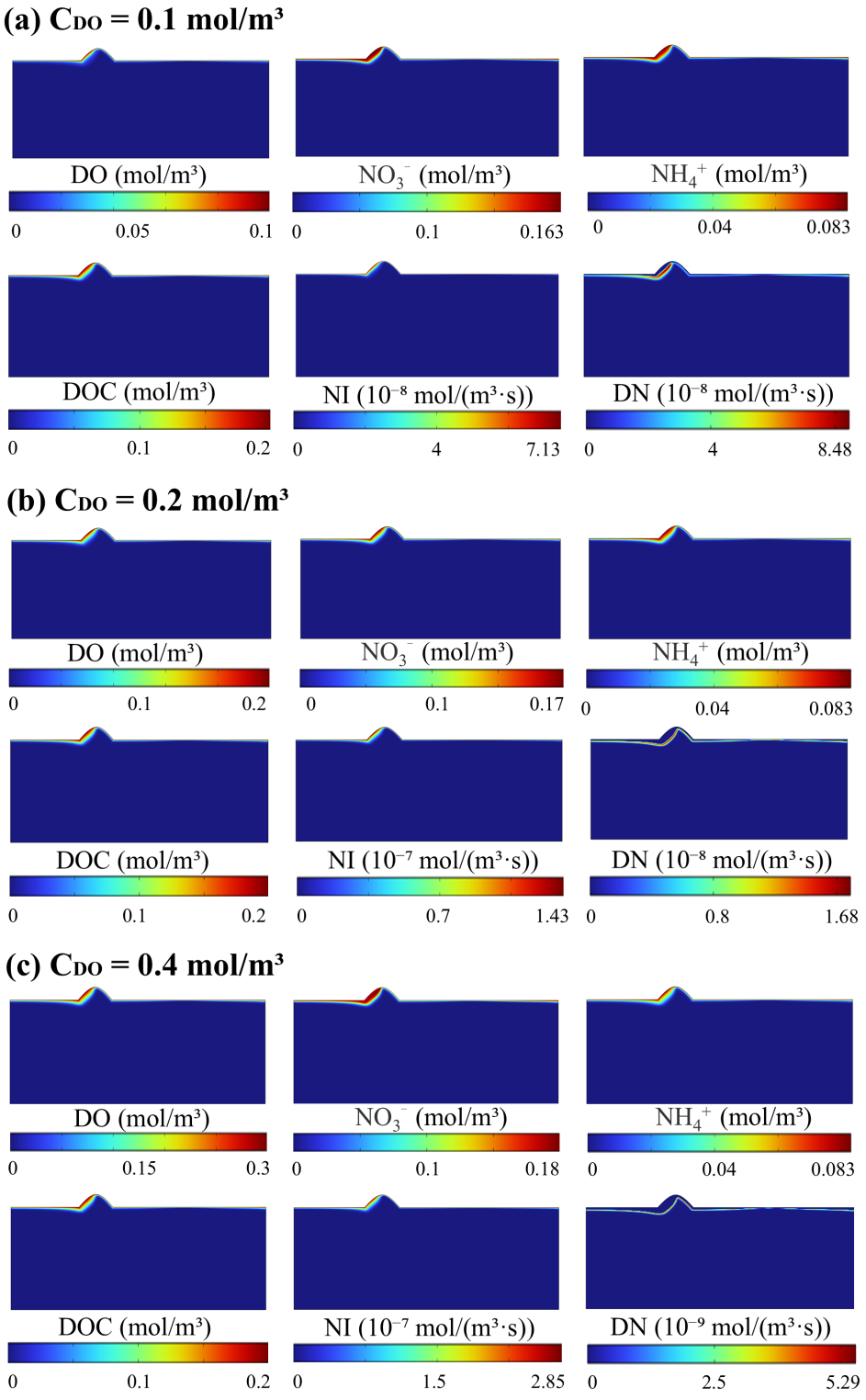

Figure 2. Distribution of four key species concentrations, and nitrification (NI) and denitrification (DN) rates with varying DO levels for the river containing the point bar.

The NI reaction is subtle and confined to the riverbank surface, while DN occurs deeper within the oxygen-depleted riverbank, exhibiting an irregular band distribution. DN reaction hotspots are located deeper within the point bar or downstream along the riverbank, often in the central area of the reaction zone (Figure 2). The trends in these reactions further indicate that NI dominates in aerobic zones, whereas DN prevails in anoxic zones. The abundance of NH_4^+ and DO causes the NI rate to peak near the WSI, then decrease with depth as these reactants are consumed. The DN rate peaks just below the anoxic–aerobic boundary and then rapidly decreases with depth, forming a narrow yet distinct DN zone.

As DO concentration increases, the four solutes (DO, NO_3^-, NH_4^+, and DOC) display varying expansion or contraction patterns (Figure 2). The penetration depth and concentration distribution of DOC change slightly, with a maximum concentration of 0.2 mol/m^3 at the interface. As penetration continues, DOC concentration gradually decreases, reaching a maximum penetration depth of approximately 0.6 m below the point bar surface. A distinct concentration stratification emerges in the middle of the bar, suggesting that NI and AR (aerobic respiration) have consumed DOC, yet DOC remains abundant overall.

In this study, DO acts solely as a reactant. Thus, under the three DO conditions, the maximum interface concentrations of DO are 0.1, 0.2, and 0.4 mol/m^3, respectively. The migration depth of DO increases with higher interface concentrations, yet it exhibits the least migration among the four solutes.

As DO increases, a significant reduction in NH_4^+ permeation along the riverbank is observed, suggesting that DO enhances nitrification, leading to increased consumption of NH_4^+.

Under these three DO scenarios, the distribution of NO_3^- remains largely unchanged, with a maximum penetration depth of 0.8 m below the junction of the left side of the bar and the riverbank. The peak concentration is not at the WSI but in the middle of the red permeation zone (Figure 2). This shift is due to NI initiated by DO and NH_4^+ during their permeation into the bar, which supplements NO_3^-, exceeding the interface concentration of 0.16 mol/m^3. As DO increases, the maximum NO_3^- concentration also changes, from 0.163 to 0.18 mol/m^3. The apparent color stratification of NO_3^- concentration at a depth of 0.1 m-0.5 m along the riverbank is primarily due to significant NO_3^- consumption via DN reaction at that location.

As the DO concentration increases from 0.1 mol/m^3 to 0.4 mol/m^3, the maximum NI rate increases from 7.13×10^{-8} to 2.85×10^{-7} mol/(m^3·s) and occurs at the WSI. The maximum reaction rate depends solely on temperature and substrate concentration. Therefore, the increase in maximum DO concentration, one of the substrates required for NI, leads to an increase in the maximum reaction rate of NI, leads to an increase in the maximum reaction rate of NI. As DO penetration depth increases, the DN reaction zone extends gradually into deeper layers of the riverbank, where substrate concentrations are lower. Consequently, the frequency of reaction hotspots (red reaction zone) decreases, and the maximum chemical reaction rate declines from 8.48×10^{-8} to 5.29×10^{-9} mol/(m^3·s).

Table 3 shows the influent and effluent amounts of key species in the nitrogen cycling process of riparian zones under different DO levels. As the concentration of DO in surface water rises, the A_{in} of DO increases from 0.22 to 0.84 mol/m while the A_{in} of other species remains largely unchanged. The A_{out} of DO significantly increases from 0.020 to 0.097 mol/m. Concurrently, due to enhanced nitrification, the A_{out} of NO_3^- rises from 0.042 to 0.046 mol/m. Under C_{DO} conditions of 0.1 mol/m^3, 0.2 mol/m^3, and 0.4 mol/m^3, the amounts of NO_3^- consumed by DN are 0.022 mol/m, 0.0064 mol/m, and 0.0019 mol/m, respectively, showing a decreasing trend. This suggests that increasing DO inhibits the progress of DN (Figure 2).

Table 3. Influent and effluent amounts of key species in the nitrogen cycling process of riparian zones under different DO levels.

Case	Species	A_{in} (mol/m)	A_{out} (mol/m)	ΔA (mol/m)	N_{DN} (mol/m)
C_{DO} = 0.1 mol/m^3	DO	0.220	0.020	0.200	0.022
	NO_3^-	0.320	0.042	0.278	
	NH_4^+	0.170	0.022	0.148	
	DOC	0.420	0.045	0.375	
C_{DO} = 0.2 mol/m^3	DO	0.430	0.042	0.178	0.0064
	NO_3^-	0.320	0.045	0.275	
	NH_4^+	0.170	0.021	0.149	
	DOC	0.420	0.045	0.375	
C_{DO} = 0.4 mol/m^3	DO	0.840	0.097	0.123	0.0019
	NO_3^-	0.320	0.046	0.274	
	NH_4^+	0.170	0.020	0.150	
	DOC	0.420	0.045	0.375	

3.2. Effect of Temperature on Nitrogen Transport and Reaction

Figure 3 illustrates the distribution of four species concentrations and the rates of NI and DN reactions in the riparian zone under three temperature conditions. The intrusion patterns of the solutes resemble those described in Section 3.1, with the deepest penetration occurring beneath the junction of the left side of the bar and the straight shore.

At T = 5 °C, the migration depths of the four solutes are nearly identical, ranging from 0.1 to 0.8 m beneath the bank. Distinct color bands of NI and DN reactions are visible, with pronounced red reaction hotspots. Under this condition, the NI reaction zone spans half of the point bar (Figure 3).

However, as the temperature rises to 25 °C, the penetration of the four solutes significantly decreases due to faster reactions and more rapid consumption of solutes. For instance, at T = 5 °C, DO nearly penetrates two-thirds of the point bar; at T = 15 °C, its presence is mainly limited to the shallow areas on the left side; and at T = 25 °C, its penetration extent is minimal and can be disregarded. As temperatures rise, the migration depth of NH_4^+ remains relatively unchanged; however, the area of peak concentration (red zones) drastically decreases to about one-tenth of its initial extent. The penetration depth of DOC decreases from an initial 0.8 m to approximately 0.5 m, with the area of peak concentration shrinking to a quarter of its original size. In summary, the migration and dispersion of various solutes are influenced differently by temperature. Generally, the infiltration depth of solutes decreases with increasing temperature (Figure 3).

In the numerical model of this study, a limiting DO concentration of 1 mg/L (0.03125 mol/m^3) is defined as the aerobic–anoxic boundary. If DO concentration exceeds this threshold, NI occurs (assuming sufficient NH_4^+), whereas DN occurs if it falls below this threshold. The shift in NO_3^- concentration from "red" to "green" in Figure 3 signifies the boundary between aerobic and anoxic conditions, marking the demarcation between NI and DN.

NO_3^- changes are primarily characterized by two aspects. First, its maximum concentration occurs just above the boundary between anoxic and hypoxic zones (Figure 3). Additionally, owing to the positive effect of higher temperatures on the nitrification rate, this maximum concentration rises with increasing temperatures (from 0.161 mol/m^3 to 0.18 mol/m^3). Conversely, temperature changes affect the distribution and migration depth of NO_3^-. As temperatures rise, the area of high NO_3^- concentration decreases, along with a slight reduction in its migration depth. Moreover, at the same temperature, the penetration depth of NO_3^- is nearly equal to that of NH_4^+.

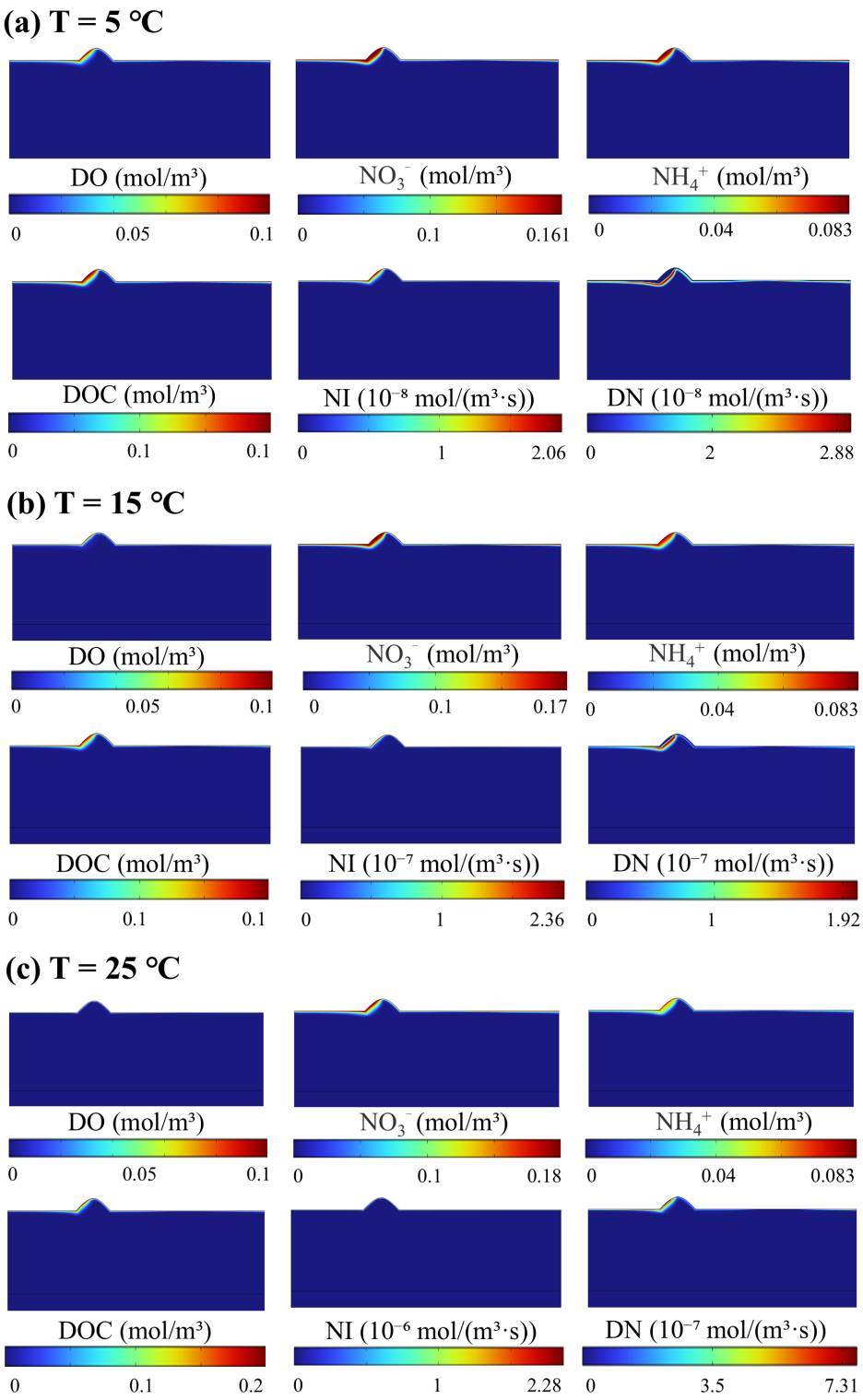

Figure 3. Distribution of four key species concentrations, and nitrification (NI) and denitrification (DN) rates with varying temperatures for the river containing the point bar.

As the temperature rises from 5 °C to 25 °C, the reactive range of NI shrinks to just 10% of its original extent. Similar to the pattern observed with DO, the maximum NI reaction depth decreases from 1 m below the riverbank to 0.2 m in the shallow left side of the point bar. At T = 5 °C, the DN reaction band is clearly visible, located below the aerobic–anoxic interface. DN hotspots exhibit a striking parabolic distribution, clearly evident at depths of 0.3–0.6 m beneath the riverbank. At T = 15 °C, the DN zone shifts upward,

revealing reactive hotspots in the central region of the riverbank. At T = 25 °C, the entire DN process moves closer to the riverbank surface, with a contracted reaction area primarily concentrated in the left-middle region. The DN hotspots are less distinct, located 0.2 m beneath the left side of the riverbank. Importantly, reduced denitrification coverage does not correspond to a decreased quantity of nitrate removal. Increased temperature promotes more vigorous chemical reactions, resulting in the rapid consumption of significant nitrate quantities through DN. Furthermore, the reduced substrate concentration inhibits the continuation of the reaction. As temperature rises from 5 °C to 25 °C, the peak NI reaction rate increases from 2.06×10^{-8} mol/(m^3·s) to 2.28×10^{-6} mol/(m^3·s). The maximum DN rate increases from 2.88×10^{-7} mol/(m^3·s) to 7.31×10^{-7} mol/(m^3·s). Both rates exhibit an upward trend as the temperature increases. This is attributed to the temperature sensitivity of the reaction rate constants. As temperature rises, the reaction rate constant increases, significantly amplifying the reaction rate.

Table 4 shows the influent and effluent amounts of key species in the nitrogen-cycling process of riparian zones with varying temperatures. With rising temperature, the A_{out} of NH_4^+ and DOC gradually decrease. The A_{out} of DO initially increases from 0.022 to 0.043 mol/m, then decreases to 0.017 mol/m, while the A_{out} of NO_3^- shows an initial decrease followed by an increase (decreased from 0.043 to 0.016, then increased to 0.048 mol/m).

Table 4. Influent and effluent amounts of key species in the nitrogen cycling process of riparian zones with varying temperatures.

Case	Species	A_{in} (mol/m)	A_{out} (mol/m)	ΔA (mol/m)	N_{DN} (mol/m)
T = 5 °C	DO	0.220	0.022	0.198	0.012
	NO_3^-	0.320	0.043	0.277	
	NH_4^+	0.170	0.022	0.148	
	DOC	0.420	0.048	0.372	
T = 15 °C	DO	0.220	0.043	0.177	0.041
	NO_3^-	0.320	0.016	0.304	
	NH_4^+	0.170	0.021	0.149	
	DOC	0.420	0.041	0.379	
T = 25 °C	DO	0.220	0.017	0.203	0.160
	NO_3^-	0.320	0.048	0.272	
	NH_4^+	0.170	0.017	0.153	
	DOC	0.420	0.029	0.391	

Higher temperatures significantly enhance nitrate removal quantities. As T rises from 5 °C to 25 °C, the N_{DN} increases from 0.012 to 0.160 mol/m (Table 4). This substantial increase is attributed to the elevated DN reaction rates (Figure 3). Comparatively, DN is more sensitive to temperature variations than to DO fluctuations (Tables 3 and 4).

4. Discussion

4.1. Effect of DO in Nitrogen Removal

In nitrogen cycling and removal mechanisms within river ecosystems, dissolved oxygen (DO) and temperature are key environmental variables that significantly influence nitrogen removal processes. Removal processes depend on several microbial-mediated transformations, including nitrification, denitrification, adsorptive sedimentation, and plant assimilation [65,66].

DO, as a direct participant in redox reactions, significantly influences the nitrification process in rivers. Nitrification is an aerobic process consisting of two stages: ammonia oxidation, performed by ammonia-oxidizing bacteria to convert ammonia to nitrite, and nitrite oxidation, carried out by nitrite-oxidizing bacteria to transform nitrite into nitrate [67,68]. This process is enhanced at higher DO levels, as an adequate supply of oxygen is essential for the biochemical reaction [69]. Conversely, in river segments with low DO levels, nitrification

may be significantly inhibited, resulting in ammonium accumulation, which adversely affects water quality [70,71].

In denitrification, low DO concentrations create an ideal anaerobic environment [72]. Denitrifying bacteria utilize nitrates as electron acceptors instead of oxygen, reducing nitrates to gaseous forms such as nitrogen gas or nitrous oxide, thereby releasing nitrogen from the aquatic system into the atmosphere [73,74]. Consequently, enhanced denitrification occurs in environments with reduced DO concentrations, facilitating nitrogen removal in riverine systems [75].

In addition to directly influencing microbial-mediated nitrogen removal, DO indirectly affects the nitrogen cycle by impacting photosynthesis rates in river ecosystems [76]. Photosynthesis can elevate DO levels in water bodies during the day and directly assimilate nitrogen through plant growth [77,78].

Our findings indicate that changes in DO significantly affect nitrogen transport and reaction processes in rivers. An increase in DO concentration within a certain range can enhance the nitrification (NI) reaction rate and reduce the denitrification (DN) reaction rate, potentially hindering nitrate removal throughout the river system. This trend is supported by research conducted by Peng et al. [79], which demonstrated that the nitrogen removal rate decreased from 50.65% to 35.22% when DO concentration was reduced from 0.125 mol/m^3 to 0.03125 mol/m^3. Research by O'Connor and Hondzo [15] and Rysgaard et al. [80] suggests that high DO concentrations inhibit the activity of denitrifying microorganisms in riverbed sediments, significantly affecting redox reaction production and leading to changes in nitrogen form transformations.

4.2. Effect of Temperature in Nitrogen Removal

Temperature affects nitrification and denitrification by regulating microbial metabolism and enzyme kinetics [81,82]. Increased temperature generally accelerates microbial metabolism, thereby enhancing nitrification. However, when temperature exceeds the viable range for microbes, excessive heat can suppress microbial activity, slowing nitrification [83]. For denitrification, rising temperatures typically increase denitrification rates, as elevated temperatures stimulate denitrifying bacteria's physiological activities. However, under extreme temperatures, enzyme inactivation may hinder denitrification, limiting nitrogen removal efficiency [84,85].

Within optimal temperature ranges, photosynthesis rates and plant growth increase, promoting nitrogen removal [86]. However, extremely high temperatures may suppress plant growth and photosynthesis, reducing nitrogen removal efficiency [87].

Our study shows that a temperature increase from 5 °C to 25 °C significantly boosts nitrification and denitrification. At 25 °C, compared to 5 °C, the peak nitrification rate increased by 110-fold, denitrification by 25-fold, and final nitrogen removal by 13-fold. Mechanistically, higher temperatures accelerate the metabolic rate and growth of denitrifying microorganisms, facilitating nitrogen conversion [88,89]. It is crucial to recognize that the depth of chemical reaction transport and solute dispersion does not directly indicate denitrification effectiveness. For example, as the temperature rises, reaction rates increase, consuming solutes before they penetrate deeper layers and hindering deeper reactions (Figure 3). Overall, the results show enhanced nitrogen removal efficiency (Table 4). Thus, accurately assessing denitrification effectiveness requires comprehensive quantitative analysis.

Our findings align with the HZ model proposed by Zheng et al. [47], which examines nitrogen migration and transformation in the HZ across seven temperatures. The model suggests that higher-temperature rivers exhibit stronger denitrification capacity than colder ones; for example, nitrogen removal at 35 °C reached 48%, compared to 28% at 5 °C.

4.3. Limitations of This Study

In natural rivers, the delivery of dissolved oxygen (DO) to riverbanks is a complex process, involving not only percolation from river water [90,91] but also replenishment from the atmosphere and the unsaturated zone of riverbanks [92,93]. These three supply pathways interact and may change their contribution sequence depending on environmen-

tal factors [29]. For example, increased river flow speed or water levels raise the river's DO contribution and reduce contributions from the atmosphere and unsaturated zone [29]. The simplified model in this study does not consider these factors, nor does it account for periodic temperature changes. Temperature can fluctuate significantly within 24 h, often exceeding a 10 °C difference, impacting chemical reactions in riverbank zones and affecting denitrification outcomes [48,94,95]. This study does not consider the interaction between temperature and DO in nitrogen removal, despite the temperature's effect on oxygen concentration. High temperatures reduce oxygen solubility and stimulate organic compound mineralization, decreasing oxygen concentrations. Reduced DO at higher temperatures can limit nitrification, while high DO levels at lower temperatures may not significantly enhance nitrification rates [96–98].

5. Conclusions

Point bars are hotspots for nitrification and denitrification in riparian zones. DO and temperature are key factors controlling nitrogen biogeochemical reactions. This study developed a model to assess nitrogen transport and reactions in a river's point bar under varying DO and temperature conditions. The model considers three nitrogen transformation pathways: aerobic respiration, nitrification, and denitrification. This study analyzed solute migration and chemical reaction patterns in a riparian zone with point bars during river flow. The simulation results indicate that increased DO drives denitrification deeper into the riverbank, enhances nitrification rates, and weakens denitrification, which is unfavorable for nitrate removal in riparian zones. Increased temperature significantly enhances denitrification, reduces nutrient penetration depth into the riverbank, and accelerates nitrogen transformation, markedly increasing nitrate removal in rivers. Future studies should delve deeper into the intricate processes of DO provision, cyclical temperature variations, and their collective impact on denitrification in riparian zones. The research outcomes could enhance our understanding of nitrogen removal and water quality enhancement in rivers.

Author Contributions: Conceptualization and Validation, X.S. and Y.L.; Software, X.S.; Formal analysis, Y.L., J.F. and D.L.; Writing—Original Draft, X.S.; Writing—Reviewing and Editing, Y.L.; Methodology, X.S., Z.L. and H.X.; Funding acquisition, Y.L. and Q.Y. All authors have read and agreed to the published version of the manuscript.

Funding: The researchers were granted funding from the National Natural Science Foundation of China (Grant Nos. 52179131 and U2040220) and the Geological Research Project of the Guizhou Bureau of Geology and Mineral Exploration and Development (No. 18, 2021). The authors express their gratitude for the support they received.

Institutional Review Board Statement: Not applicable.

Informed Consent Statement: Not applicable.

Data Availability Statement: The data presented in this study are available on request from the corresponding author. The data are not publicly available due to privacy restrictions.

Conflicts of Interest: The authors declare no conflicts of interest.

References

1. Cardenas, M.B. The effect of river bend morphology on flow and timescales of surface water–groundwater exchange across pointbars. *J. Hydrol.* **2008**, *362*, 134–141. [CrossRef]
2. Storey, R.G.; Howard, K.W.; Williams, D.D. Factors controlling riffle-scale hyporheic exchange flows and their seasonal changes in a gaining stream: A three-dimensional groundwater flow model. *Water Resour. Res.* **2003**, *39*, 1034. [CrossRef]
3. Hall, R.J.O.; Baker, M.A.; Arp, C.D.; Koch, B.J. Hydrologic control of nitrogen removal, storage, and export in a mountain stream. *Limnol. Oceanogr.* **2009**, *54*, 2128–2142. [CrossRef]
4. Kasahara, T.; Hill, A.R. Hyporheic exchange flows induced by constructed riffles and steps in lowland streams in southern Ontario, Canada. *Hydrol. Process. Int. J.* **2006**, *20*, 4287–4305. [CrossRef]
5. Marzadri, A.; Tonina, D.; Bellin, A.; Vignoli, G.; Tubino, M. Semianalytical analysis of hyporheic flow induced by alternate bars. *Water Resour. Res.* **2010**, *46*, W07531. [CrossRef]

6. Lowell, J.L.; Gordon, N.; Engstrom, D.; Stanford, J.A.; Holben, W.E.; Gannon, J.E. Habitat heterogeneity and associated microbial community structure in a small-scale floodplain hyporheic flow path. *Microb. Ecol.* **2009**, *58*, 611–620. [CrossRef]
7. Seitzinger, S.; Harrison, J.A.; Böhlke, J.; Bouwman, A.; Lowrance, R.; Peterson, B.; Tobias, C.; Drecht, G.V. Denitrification across landscapes and waterscapes: A synthesis. *Ecol. Appl.* **2006**, *16*, 2064–2090. [CrossRef]
8. Khan, N.; Jhariya, M.K.; Banerjee, A.; Meena, R.S.; Raj, A.; Yadav, S.K. Riparian conservation and restoration for ecological sustainability. In *Natural Resources Conservation and Advances for Sustainability*; Elsevier: Amsterdam, The Netherlands, 2022; pp. 195–216.
9. Seavy, N.E.; Gardali, T.; Golet, G.H.; Griggs, F.T.; Howell, C.A.; Kelsey, R.; Small, S.L.; Viers, J.H.; Weigand, J.F. Why climate change makes riparian restoration more important than ever: Recommendations for practice and research. *Ecol. Restor.* **2009**, *27*, 330–338. [CrossRef]
10. Urbanič, G.; Politti, E.; Rodríguez-González, P.M.; Payne, R.; Schook, D.; Alves, M.H.; Anđelković, A.; Bruno, D.; Chilikova-Lubomirova, M.; Di Lonardo, S. Riparian zones—From policy neglected to policy integrated. *Front. Environ. Sci.* **2022**, *10*, 868527. [CrossRef]
11. Hao, Z.-L.; Ali, A.; Ren, Y.; Su, J.-F.; Wang, Z. A mechanistic review on aerobic denitrification for nitrogen removal in water treatment. *Sci. Total Environ.* **2022**, *847*, 157452. [CrossRef]
12. Alexander, R.B.; Böhlke, J.K.; Boyer, E.W.; David, M.B.; Harvey, J.W.; Mulholland, P.J.; Seitzinger, S.P.; Tobias, C.R.; Tonitto, C.; Wollheim, W.M. Dynamic modeling of nitrogen losses in river networks unravels the coupled effects of hydrological and biogeochemical processes. *Biogeochemistry* **2009**, *93*, 91–116. [CrossRef]
13. Grischek, T.; Hiscock, K.; Metschies, T.; Dennis, P.; Nestler, W. Factors affecting denitrification during infiltration of river water into a sand and gravel aquifer in Saxony, Germany. *Water Res.* **1998**, *32*, 450–460. [CrossRef]
14. Burgin, A.J.; Groffman, P.M.; Lewis, D.N. Factors regulating denitrification in a riparian wetland. *Soil Sci. Soc. Am. J.* **2010**, *74*, 1826–1833. [CrossRef]
15. O'Connor, B.L.; Hondzo, M. Enhancement and inhibition of denitrification by fluid-flow and dissolved oxygen flux to stream sediments. *Environ. Sci. Technol.* **2008**, *42*, 119–125. [CrossRef] [PubMed]
16. Klocker, C.A.; Kaushal, S.S.; Groffman, P.M.; Mayer, P.M.; Morgan, R.P. Nitrogen uptake and denitrification in restored and unrestored streams in urban Maryland, USA. *Aquat. Sci.* **2009**, *71*, 411–424. [CrossRef]
17. Veraart, A.J.; Audet, J.; Dimitrov, M.R.; Hoffmann, C.C.; Gillissen, F.; de Klein, J.J. Denitrification in restored and unrestored Danish streams. *Ecol. Eng.* **2014**, *66*, 129–140. [CrossRef]
18. Her, J.-J.; Huang, J.-S. Influences of carbon source and C/N ratio on nitrate/nitrite denitrification and carbon breakthrough. *Bioresour. Technol.* **1995**, *54*, 45–51. [CrossRef]
19. Ge, S.; Peng, Y.; Wang, S.; Lu, C.; Cao, X.; Zhu, Y. Nitrite accumulation under constant temperature in anoxic denitrification process: The effects of carbon sources and COD/NO3-N. *Bioresour. Technol.* **2012**, *114*, 137–143. [CrossRef]
20. Alldred, M.; Baines, S.B. Effects of wetland plants on denitrification rates: A meta-analysis. *Ecol. Appl.* **2016**, *26*, 676–685. [CrossRef]
21. Šimek, M.; Cooper, J. The influence of soil pH on denitrification: Progress towards the understanding of this interaction over the last 50 years. *Eur. J. Soil Sci.* **2002**, *53*, 345–354. [CrossRef]
22. Saleh-Lakha, S.; Shannon, K.E.; Henderson, S.L.; Goyer, C.; Trevors, J.T.; Zebarth, B.J.; Burton, D.L. Effect of pH and temperature on denitrification gene expression and activity in Pseudomonas mandelii. *Appl. Environ. Microbiol.* **2009**, *75*, 3903–3911. [CrossRef]
23. Baeseman, J.; Smith, R.; Silverstein, J. Denitrification potential in stream sediments impacted by acid mine drainage: Effects of pH, various electron donors, and iron. *Microb. Ecol.* **2006**, *51*, 232–241. [CrossRef] [PubMed]
24. Seitzinger, S.P. Denitrification in aquatic sediments. In *Denitrification in Soil and Sediment*; Springer: Berlin/Heidelberg, Germany, 1990; pp. 301–322.
25. Deutsch, B.; Forster, S.; Wilhelm, M.; Dippner, J.; Voss, M. Denitrification in sediments as a major nitrogen sink in the Baltic Sea: An extrapolation using sediment characteristics. *Biogeosciences* **2010**, *7*, 3259–3271. [CrossRef]
26. Saunders, D.; Kalff, J. Denitrification rates in the sediments of Lake Memphremagog, Canada–USA. *Water Res.* **2001**, *35*, 1897–1904. [CrossRef] [PubMed]
27. Boynton, W.R.; Kemp, W.M. Nutrient regeneration and oxygen consumption by sediments along an estuarine salinity gradient. *Mar. Ecol. Prog. Ser. Oldendorf* **1985**, *23*, 45–55. [CrossRef]
28. Cornwell, J.C.; Kemp, W.M.; Kana, T.M. Denitrification in coastal ecosystems: Methods, environmental controls, and ecosystem level controls, a review. *Aquat. Ecol.* **1999**, *33*, 41–54. [CrossRef]
29. Bu, X.; Dai, H.; Yuan, S.; Zhu, Q.; Li, X.; Zhu, Y.; Li, Y.; Wen, Z. Model-based analysis of dissolved oxygen supply to aquifers within riparian zones during river level fluctuations: Dynamics and influencing factors. *J. Hydrol.* **2021**, *598*, 126460. [CrossRef]
30. Reeder, W.J.; Quick, A.M.; Farrell, T.B.; Benner, S.G.; Feris, K.P.; Tonina, D. Spatial and temporal dynamics of dissolved oxygen concentrations and bioactivity in the hyporheic zone. *Water Resour. Res.* **2018**, *54*, 2112–2128. [CrossRef]
31. Greig, S.; Sear, D.; Carling, P. A review of factors influencing the availability of dissolved oxygen to incubating salmonid embryos. *Hydrol. Process. Int. J.* **2007**, *21*, 323–334. [CrossRef]
32. Tonina, D.; Buffington, J.M. A three-dimensional model for analyzing the effects of salmon redds on hyporheic exchange and egg pocket habitat. *Can. J. Fish. Aquat. Sci.* **2009**, *66*, 2157–2173. [CrossRef]

33. Zarnetske, J.P.; Haggerty, R.; Wondzell, S.M.; Baker, M.A. Labile dissolved organic carbon supply limits hyporheic denitrification. *J. Geophys. Res.* **2011**, *116*, G04036. [CrossRef]
34. Stanford, G.; Dzienia, S.; Vander Pol, R.A. Effect of temperature on denitrification rate in soils. *Soil Sci. Soc. Am. J.* **1975**, *39*, 867–870. [CrossRef]
35. Pfenning, K.; McMahon, P. Effect of nitrate, organic carbon, and temperature on potential denitrification rates in nitrate-rich riverbed sediments. *J. Hydrol.* **1997**, *187*, 283–295. [CrossRef]
36. Zhang, H.; Liu, K.; Huang, T.; Li, N.; Si, F.; Feng, J.; Huang, X.; Miao, Y. Effect of thermal stratification on denitrifying bacterial community in a deep drinking water reservoir. *J. Hydrol.* **2021**, *596*, 126090. [CrossRef]
37. Jayakumar, A.; O'mullan, G.; Naqvi, S.; Ward, B.B. Denitrifying bacterial community composition changes associated with stages of denitrification in oxygen minimum zones. *Microb. Ecol.* **2009**, *58*, 350–362. [CrossRef]
38. Tall, L.; Caraco, N.; Maranger, R. Denitrification hot spots: Dominant role of invasive macrophyte Trapa natans in removing nitrogen from a tidal river. *Ecol. Appl.* **2011**, *21*, 3104–3114. [CrossRef]
39. Martin, T.L.; Kaushik, N.; Trevors, J.; Whiteley, H. Denitrification in temperate climate riparian zones. *Water Air Soil Pollut.* **1999**, *111*, 171–186. [CrossRef]
40. Nimick, D.A.; Gammons, C.H.; Cleasby, T.E.; Madison, J.P.; Skaar, D.; Brick, C.M. Diel cycles in dissolved metal concentrations in streams: Occurrence and possible causes. *Water Resour. Res.* **2003**, *39*, 1247. [CrossRef]
41. Herrman, K.S.; Bouchard, V.; Moore, R.H. Factors affecting denitrification in agricultural headwater streams in Northeast Ohio, USA. *Hydrobiologia* **2008**, *598*, 305–314. [CrossRef]
42. Zhang, Q.; Chen, X.; Luo, W.; Wu, H.; Liu, X.; Chen, W.; Tang, J.; Zhang, L. Effects of temperature on the characteristics of nitrogen removal and microbial community in post solid-phase denitrification biofilter process. *Int. J. Environ. Res. Public Health* **2019**, *16*, 4466. [CrossRef]
43. Ji, B.; Yang, K.; Zhu, L.; Jiang, Y.; Wang, H.; Zhou, J.; Zhang, H. Aerobic denitrification: A review of important advances of the last 30 years. *Biotechnol. Bioprocess Eng.* **2015**, *20*, 643–651. [CrossRef]
44. Seitzinger, S.P. Linkages between organic matter mineralization and denitrification in eight riparian wetlands. *Biogeochemistry* **1994**, *25*, 19–39. [CrossRef]
45. Thamdrup, B.; Fleischer, S. Temperature dependence of oxygen respiration, nitrogen mineralization, and nitrification in Arctic sediments. *Aquat. Microb. Ecol.* **1998**, *15*, 191–199. [CrossRef]
46. Bardini, L.; Boano, F.; Cardenas, M.; Revelli, R.; Ridolfi, L. Nutrient cycling in bedform induced hyporheic zones. *Geochim. Et Cosmochim. Acta* **2012**, *84*, 47–61. [CrossRef]
47. Zheng, L.; Cardenas, M.B.; Wang, L. Temperature effects on nitrogen cycling and nitrate removal-production efficiency in bed form-induced hyporheic zones. *J. Geophys. Res. Biogeosciences* **2016**, *121*, 1086–1103. [CrossRef]
48. Zheng, L.; Bayani Cardenas, M. Diel stream temperature effects on nitrogen cycling in hyporheic zones. *J. Geophys. Res. Biogeosciences* **2018**, *123*, 2743–2760. [CrossRef]
49. Shuai, P.; Cardenas, M.B.; Knappett, P.S.; Bennett, P.C.; Neilson, B.T. Denitrification in the banks of fluctuating rivers: The effects of river stage amplitude, sediment hydraulic conductivity and dispersivity, and ambient groundwater flow. *Water Resour. Res.* **2017**, *53*, 7951–7967. [CrossRef]
50. Song, X.; Liu, Y.; Liu, D.; Feng, J.; Li, L.; Guo, Y.; Luo, J.; Jiang, W. Influence of point bars on nitrogen transport and reaction in riparian zones. *J. Hydrol.* **2024**, *637*, 131388. [CrossRef]
51. Zhou, T.; Endreny, T. The straightening of a river meander leads to extensive losses in flow complexity and ecosystem services. *Water* **2020**, *12*, 1680. [CrossRef]
52. Birnir, B. Turbulent rivers. *Q. Appl. Math.* **2008**, *66*, 565–594. [CrossRef]
53. Myong, H.K.; Kasagi, N. A new approach to the improvement of k-ε turbulence model for wall-bounded shear flows. *JSME Int. J. Ser. 2 Fluids Eng. Heat Transf. Power Combust. Thermophys. Prop.* **1990**, *33*, 63–72. [CrossRef]
54. Mohammadi, B.; Pironneau, O. Analysis of The k-Epsilon Turbulence Model. 1993. Available online: https://www.ljll.fr/pironneau/publi/publications/bookBMOPke.pdf (accessed on 24 July 2024).
55. Janssen, F.; Cardenas, M.B.; Sawyer, A.H.; Dammrich, T.; Krietsch, J.; Beer, D.J.D. A comparative experimental and multiphysics computational fluid dynamics study of coupled surface–subsurface flow in bed forms. *Water Resour. Res.* **2012**, *48*, W08514. [CrossRef]
56. Dagan, G. The generalization of Darcy's law for nonuniform flows. *Water Resour. Res.* **1979**, *15*, 1–7. [CrossRef]
57. Whitaker, S. Flow in porous media I: A theoretical derivation of Darcy's law. *Transp. Porous Media* **1986**, *1*, 3–25. [CrossRef]
58. Zarnetske, J.P.; Haggerty, R.; Wondzell, S.M.; Bokil, V.A.; González-Pinzón, R. Coupled transport and reaction kinetics control the nitrate source-sink function of hyporheic zones. *Water Resour. Res.* **2012**, *48*, W11508.
59. Wang, C.; Cheng, P. A multiphase mixture model for multiphase, multicomponent transport in capillary porous media—I. Model development. *Int. J. Heat Mass Transf.* **1996**, *39*, 3607–3618. [CrossRef]
60. Trauth, N.; Fleckenstein, J.H. Single discharge events increase reactive efficiency of the hyporheic zone. *Water Resour. Res.* **2017**, *53*, 779–798. [CrossRef]
61. Millington, R.; Quirk, J. Permeability of porous solids. *Trans. Faraday Soc.* **1961**, *57*, 1200–1207. [CrossRef]
62. Winzor, D.J.; Jackson, C.M. Interpretation of the temperature dependence of equilibrium and rate constants. *J. Mol. Recognit. Interdiscip. J.* **2006**, *19*, 389–407. [CrossRef]

63. Shah, D.B.; Coulman, G.A. Kinetics of nitrification and denitrification reactions. *Biotechnol. Bioeng.* **1978**, *20*, 43–72. [CrossRef]
64. Ping, X.; Jin, M.; Xian, Y. Effect of bioclogging on the nitrate source and sink function of a hyporheic zone. *J. Hydrol.* **2020**, *590*, 125425. [CrossRef]
65. Zhao, Y.; Xia, Y.; Ti, C.; Shan, J.; Li, B.; Xia, L.; Yan, X. Nitrogen removal capacity of the river network in a high nitrogen loading region. *Environ. Sci. Technol.* **2015**, *49*, 1427–1435. [CrossRef] [PubMed]
66. Craig, L.S.; Palmer, M.A.; Richardson, D.C.; Filoso, S.; Bernhardt, E.S.; Bledsoe, B.P.; Doyle, M.W.; Groffman, P.M.; Hassett, B.A.; Kaushal, S.S. Stream restoration strategies for reducing river nitrogen loads. *Front. Ecol. Environ.* **2008**, *6*, 529–538. [CrossRef]
67. Xia, X.; Yang, Z.; Huang, G.; Zhang, X.; Yu, H.; Rong, X. Nitrification in natural waters with high suspended-solid content—-A study for the Yellow River. *Chemosphere* **2004**, *57*, 1017–1029. [CrossRef]
68. Prosser, J.I. Autotrophic nitrification in bacteria. *Adv. Microb. Physiol.* **1990**, *30*, 125–181.
69. Dai, M.; Wang, L.; Guo, X.; Zhai, W.; Li, Q.; He, B.; Kao, S.-J. Nitrification and inorganic nitrogen distribution in a large perturbed river/estuarine system: The Pearl River Estuary, China. *Biogeosciences* **2008**, *5*, 1227–1244. [CrossRef]
70. Hsiao, S.-Y.; Hsu, T.-C.; Liu, J.-W.; Xie, X.; Zhang, Y.; Lin, J.; Wang, H.; Yang, J.-Y.; Hsu, S.-C.; Dai, M. Nitrification and its oxygen consumption along the turbid Chang Jiang River plume. *Biogeosciences* **2014**, *11*, 2083–2098. [CrossRef]
71. Gowda, T.H. Modelling nitrification effects on the dissolved oxygen regime of the Speed River. *Water Res.* **1983**, *17*, 1917–1927. [CrossRef]
72. Delwiche, C.; Bryan, B.A. Denitrification. *Annu. Rev. Microbiol.* **1976**, *30*, 241–262. [CrossRef]
73. Zhou, S.; Borjigin, S.; Riya, S.; Terada, A.; Hosomi, M. The relationship between anammox and denitrification in the sediment of an inland river. *Sci. Total Environ.* **2014**, *490*, 1029–1036. [CrossRef]
74. Hill, A. Denitrification in the nitrogen budget of a river ecosystem. *Nature* **1979**, *281*, 291–292. [CrossRef]
75. Zumft, W.G. Cell biology and molecular basis of denitrification. *Microbiol. Mol. Biol. Rev.* **1997**, *61*, 533–616.
76. Hellemann, D.; Tallberg, P.; Bartl, I.; Voss, M.; Hietanen, S. Denitrification in an oligotrophic estuary: A delayed sink for riverine nitrate. *Mar. Ecol. Prog. Ser.* **2017**, *583*, 63–80. [CrossRef]
77. Xia, X.; Zhang, S.; Li, S.; Zhang, L.; Wang, G.; Zhang, L.; Wang, J.; Li, Z. The cycle of nitrogen in river systems: Sources, transformation, and flux. *Environ. Sci. Process. Impacts* **2018**, *20*, 863–891. [CrossRef] [PubMed]
78. Baker, A.L.; Baker, K.K. Effects of temperature and current discharge on the concentration and photosynthetic activity of the phytoplankton in the upper Mississippi River. *Freshw. Biol.* **1979**, *9*, 191–198. [CrossRef]
79. Peng, B.; Liang, H.; Wang, S.; Gao, D. Effects of DO on N2O emission during biological nitrogen removal using aerobic granular sludge via shortcut simultaneous nitrification and denitrification. *Environ. Technol.* **2018**, *41*, 251–259. [CrossRef]
80. Rysgaard, S.; Risgaard-Petersen, N.; Niels Peter, S.; Kim, J.; Lars Peter, N. Oxygen regulation of nitrification and denitrification in sediments. *Limnol. Oceanogr.* **1994**, *39*, 1643–1652. [CrossRef]
81. Pina-Ochoa, E.; Álvarez-Cobelas, M. Denitrification in aquatic environments: A cross-system analysis. *Biogeochemistry* **2006**, *81*, 111–130. [CrossRef]
82. Pinay, G.; Gumiero, B.; Tabacchi, E.; Gimenez, O.; Tabacchi-Planty, A.M.; Hefting, M.M.; Burt, T.P.; Black, V.A.; Nilsson, C.; Iordache, V. Patterns of denitrification rates in European alluvial soils under various hydrological regimes. *Freshw. Biol.* **2007**, *52*, 252–266. [CrossRef]
83. García-Ruiz, R.; Pattinson, S.N.; Whitton, B.A. Denitrification and nitrous oxide production in sediments of the Wiske, a lowland eutrophic river. *Sci. Total Environ.* **1998**, *210*, 307–320. [CrossRef]
84. Braker, G.; Schwarz, J.; Conrad, R. Influence of temperature on the composition and activity of denitrifying soil communities. *FEMS Microbiol. Ecol.* **2010**, *73*, 134–148. [CrossRef] [PubMed]
85. Saad, O.A.; Conrad, R. Temperature dependence of nitrification, denitrification, and turnover of nitric oxide in different soils. *Biol. Fertil. Soils* **1993**, *15*, 21–27.
86. Pribyl, A.L.; Mccutchan, J.H.; Lewis, W.M.; Saunders Iii, J.F. Whole-system estimation of denitrification in a plains river: A comparison of two methods. *Biogeochemistry* **2005**, *73*, 439–455. [CrossRef]
87. Xie, Y.; Tilstone, G.H.; Widdicombe, C.; Woodward, E.M.S.; Harris, C.; Barnes, M.K. Effect of increases in temperature and nutrients on phytoplankton community structure and photosynthesis in the western English Channel. *Mar. Ecol. Prog. Ser.* **2015**, *519*, 61–73. [CrossRef]
88. Bonnett, S.; Blackwell, M.; Leah, R.; Cook, V.; O'connor, M.; Maltby, E. Temperature response of denitrification rate and greenhouse gas production in agricultural river marginal wetland soils. *Geobiology* **2013**, *11*, 252–267. [CrossRef]
89. Pattinson, S.N.; García-Ruiz, R.; Whitton, B.A. Spatial and seasonal variation in denitrification in the Swale–Ouse system, a river continuum. *Sci. Total Environ.* **1998**, *210*, 289–305. [CrossRef]
90. Kohfahl, C.; Massmann, G.; Pekdeger, A. Sources of oxygen flux in groundwater during induced bank filtration at a site in Berlin, Germany. *Hydrogeol. J* **2009**, *17*, 571–578. [CrossRef]
91. Berlin, M.; Kumar, G.S.; Nambi, I.M. Numerical modeling on the effect of dissolved oxygen on nitrogen transformation and transport in unsaturated porous system. *Environ. Model. Assess.* **2014**, *19*, 283–299. [CrossRef]
92. Malard, F.; Hervant, F. Oxygen supply and the adaptations of animals in groundwater. *Freshw. Biol.* **1999**, *41*, 1–30. [CrossRef]
93. Haberer, C.M.; Rolle, M.; Cirpka, O.A.; Grathwohl, P. Oxygen transfer in a fluctuating capillary fringe. *Vadose Zone J.* **2012**, *11*, vzj2011.0056. [CrossRef]

94. Dugdale, S.J.; Hannah, D.M.; Malcolm, I.A. River temperature modelling: A review of process-based approaches and future directions. *Earth-Sci. Rev.* **2017**, *175*, 97–113. [CrossRef]
95. Holmes, R.M.; Jones, J.B.; Fisher, S.G.; Grimm, N.B. Denitrification in a nitrogen-limited stream ecosystem. *Biogeochemistry* **1996**, *33*, 125–146. [CrossRef]
96. Veraart, A.J.; De Klein, J.J.; Scheffer, M. Warming can boost denitrification disproportionately due to altered oxygen dynamics. *PLoS ONE* **2011**, *6*, e18508. [CrossRef] [PubMed]
97. De Klein, J.J.; Overbeek, C.C.; Juncher Jørgensen, C.; Veraart, A.J. Effect of temperature on oxygen profiles and denitrification rates in freshwater sediments. *Wetlands* **2017**, *37*, 975–983. [CrossRef]
98. Rajesh, M.; Rehana, S. Impact of climate change on river water temperature and dissolved oxygen: Indian riverine thermal regimes. *Sci. Rep.* **2022**, *12*, 9222. [CrossRef]